Physicochem. Probl. Miner. Process., 59(1), 2023, 161679

http://www.journalssystem.com/ppmp

Physicochemical Problems of Mineral Processing

ISSN 1643-1049

Novel nanofibers composite based clay: synthesis, characterization and intrinsic properties

Youssef El Omari, Zakaria Kbiri, Bouazza Tbib, Abdelhafid Abouharim, Khalil El-Hami

Mohammed V University in Rabat, Scientific Institute, Av. Ibn Batouta BP 703, Agdal, Rabat, Morocco

Corresponding author: youyouomari@gmail.com

Abstract: This work focuses on the study of red brick doped with reed fibers. These properties have been studied using characterizations techniques. In this context, we used Fourier transform infrared spectroscopy (FTIR), scanning electron microscopy (SEM) and X-ray diffraction (XRD) analysis on the stability configuration, chemical structures and surface properties (morphology and porosity). The synthesis protocol is followed according to the manufacturing process of bricks on an industrial scale with well-defined standards and specifications. SEM and XRD experimental results showed that doping of clay fibers could effectively increase pore size and grain size as an indication of the removal of non-crystalline cellulosic materials from the fibers. The benefits of using fiber additives in clay bricks are then confirmed from a performance and environmental point of view.

Keywords: clay bricks, cellulosic fiber, composites, structural and morphological characterization

1. Introduction

Over the past decade, with the overexploitation and depletion of resources Fossil resources and severe environmental degradation are among the increased interest in developing low-cost applications and renewable resources (Bilgiç and Bilgic, 2019). Clay composites have important advantages in the development and innovation of polymers such as epoxy (Park and Jana, 2003; Messersmith, 1994), methyl methacrylate (Okamoto et al., 2001), nylon (Choi et al., 2001), polyaniline (Cheng et al., 2005), polyethylene (Lu et al., 2005) and polypropylene (Wang et al., 2007). It is well known that the parent material has a major cause of environmental pollution due to the emission of smoke during production. In addition, the non-biodegradability of synthetic polymers results in their elimination and recycling. On the other hand, natural biodegradable cellulosic fibers can be easily incorporated into composites that have improved properties and overcome the problems of climate change (Wang et al., 2007; Ray and Bousmina, 2005). Hence, a right approach is to improve and make it more cost effective material is the addition of natural fiber that have recently gained attention to ameliorate the composite matrix for based clay for their utilisation in building, because of many advantage such as low density, nonabrasive character, high specific strength, low cost and biocompatibility (Bilgiç and Bilgic, 2019; Chen et al., 2015). Various forms of cellulose have been investigated as reinforcing agent in clay. Therefore, it is necessary to use natural fibers and incorporate them into clay in order to reduce the production cost by partially replacing the clay by low cost mixture of clay and the present form of natural cellulosic fibers without destroying the biodegradation performance of the polymer matrix (Bilgiç and Bilgic , 2019; Chen et al., 2015). The composites are cellulose (Park et al., 2004; Park et al., 2006), chitosan (Wang et al., 2007 and Zhuang et al., 2007), polylactide (PLA) (Ray et al., 2003), gelatin (Li et al., 2003) and poly (3-hydroxy butyrate) (PHB) (Maiti et al., 2003). The cellulose is a molecular extracted from vegetable plants, it is a renewable polymer largely available in nature, which can be used in material applications. The annual production of cellulose biomass is about one trillion tons (Mas et al., 2005), implying the inexhaustible nature of cellulose as a natural raw material (Ioelovich, 2008). Cellulosic nanocrystals (CNCs) have been used in various types of applications such as textiles, gels, optics, aircraft, pharmaceuticals, food additives, composites, electronics, dental repair and adsorption (Mccormick, 2010). cellulose contains hydroxyl (-OH) groups on the glucose cycle acting as coordination sites with heavy metal ions, making it an attractive natural adsorbent (Ngah and Hanafiah, 2008; Thirumavalavan et al., 2009). In this study,

DOI: 10.37190/ppmp/161679

red clay doped by cellulosic fibers of reed plant, they were processed by a simple method to create a porous material in order to assess their feasibility as nanofiber reinforcing material and for developing the utilisation of red brick in many applications such as building (Kbiri et al., 2020; Kbiri et al., 2022) and other biomaterial applications. Fourier transform infrared spectroscopy (FTIR), scanning electron microscope (SEM), X-Ray fluorescence spectroscopy and X-ray diffraction (XRD) analysis were used to study the chemical structure, morphology of raw fibers and processed clay. This study aims to provide a systematic overview of how cellulosic reed plant fibers can be used to modify the porosity of red brick in the building for a novel ecological construction.

2. Experimental section

2.1. Materials

The reed plant stick as can be seen in Fig. 1, was ground using a drill with wood polishing disc, and the powder was manually collected in a plastic bag as shown in Fig. 2 shows the sample before and after grinding. Then, the samples were prepared as follows: we doped the clay with different percentages of fiber reed plant in the presence of water. Table (1) illustrates composition of the prepared products.

Fig. 1. Reed plant

Fig. 2. Crushed reed plant with clay

Table 1. Composition of the prepared products

Sample	Clay (kg)	Fibers (%)	Water (L)
Sample 1	9.75	2.5	1.75
Sample 2	9.50	5	1.75
Sample 3	9.25	7.5	1.75
Sample 4	9.0	10	1.75
Sample 5	8.5	15	1.75

2.2. Photograph of cellulosic fibers from 25°C to 825 °C

Following an experimental part and after a thermal heating to 825°C, the samples have been subjected to the brick manufacturing process in a Jbel Annour brickyard, specialist in the manufacture of red bricks. The synthesis of the samples was carried out according to the industrial protocol. The photos of our products are illustrated in the Figs. 3-4.

It is observed that the color of the samples below are remarkable. This color is because of the elements that make up this present brick. We also observe a circular gray color in the interior part of the brig and that its exterior part remains red. This aspect is the fingerprint of cellulosic fibers like tree rings. When the percentage of fiber has increased, the diameter of ring increase as shown in Fig. 5. These differences present intrinsic properties of fibers of reed plant used.

Fig. 3. Photograph of samples of clay doped by reed plant fibers at 25°C

Fig. 4. Photograph of red brick doped by reed plant fibers at 825°C

Fig. 5 represents the difference between the samples. Resistance of fiber varies considerably depending on the direction of the applied force, i.e. parallel, radial or tangential to the grain of the wood. Wood is strongest when stressed in the direction of the grain, in tension or in compression.

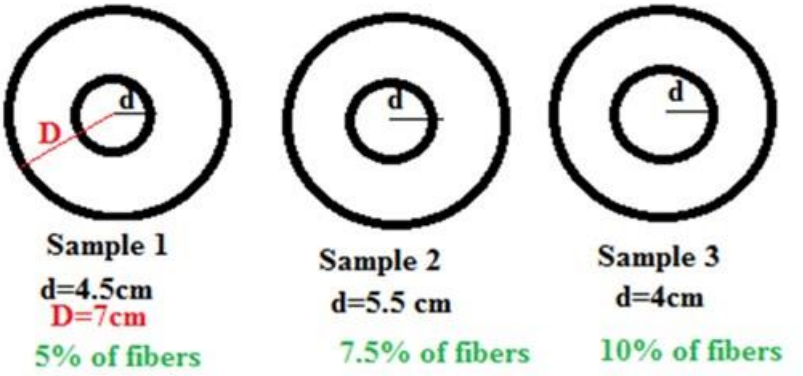

Fig. 5. Drawing describes the difference between the samples

3. Results and discussion

3.1. Fourier transform infrared (FTIR) spectroscopy

FTIR spectra were taken using a Perkin Elmer Frontier FTIR spectrometer. The scanning range was from 600 to 4000 cm^{-1} with a spectral resolution of 4 cm^{-1} and 33 scans. A few milligrams of each product were taken, and they measured directly by FT-IR spectrometer UATR. The FTIR experiments results are show in Fig. 6. The broad peak ranging from 3660 to 2990 cm^{-1} was because of hydroxyl groups stretching vibration present in cellulose, hemicellulose, and lignin. The vibration peaks at 2919 cm^{-1} and 2854 cm^{-1} revealed asymmetric and symmetric CH_2 stretching in cellulose/hemicellulose, respectively. The peaks at 1730 cm^{-1}, 1620 cm^{-1}, 1245 cm^{-1} and 1023 cm^{-1} corresponded to ester carbonyl group stretching, C=O stretching in carboxylic acid in cellulose, O-CH_3 stretching in lignin and C–O stretching vibration (Oushabi et al., 2018; Atiqah et al., 2018; Minhajul et al., 2017). The clay mineral samples shown in Fig. 5 can be attributed to kaolinite by IR transmittance spectra. Their IR spectra demonstrate fully-represented and well-resolved Si-O-Si and Al-O-Si bands of the mineral lattice, as shown in Table 2 (Smilja et al., 2003). From the FT-IR spectrum, it is clear that the clay and cellulosic fiber peaks are visible as can be seen in Fig. 5. Major peaks like the alkane peak due to the presence of the alkyl group in the modified clay, they are finding at 9000-1020 cm^{-1} (Chen et al., 2015). From 1000.15 cm^{-1} to 1020.87cm^{-1} due to C-H trans waggin vibration present in the crystalline cellulose can be observed in the composite, the bridge Si-O-Si, Si-O stretching of clay structure. The band about 446 cm^{-1} assigned to lattice vibrations. These peaks are particularly dominant in the samples S1, S2, S3 and S4; the peaks of clay and fibers overlapped. The displacement of the main peak position due to the effect of the addition of fibers.

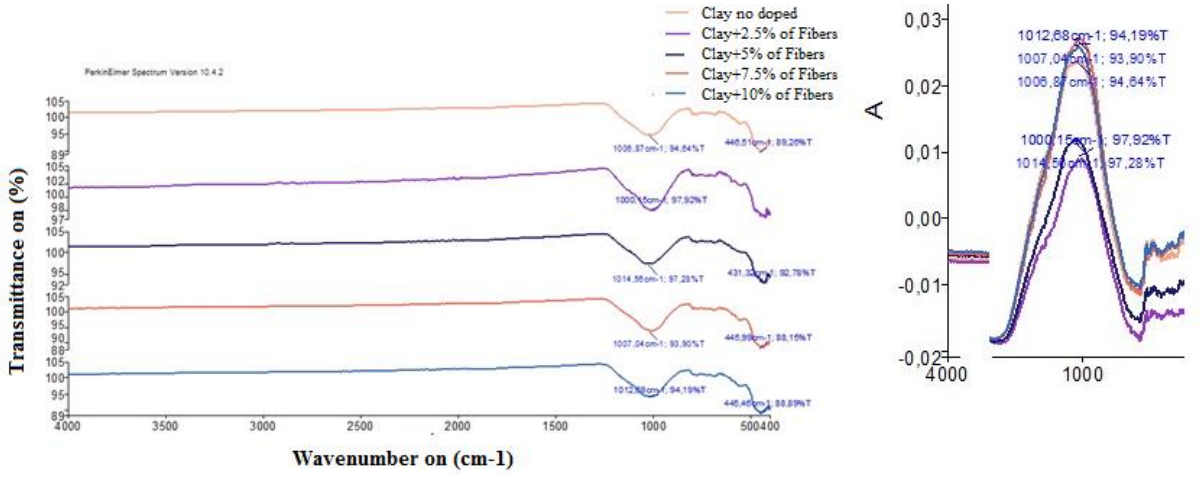

Fig. 6. FTIR spectra for (A) raw clay and clay doped by fibers from 2.5% to 10%

Peaks resulting from the combination of these elements can be observed. While in the S1 composite, the clay and fiber peaks are more evident individually, in the S5 composite, the peaks are more distorted. This implies a better interaction between the clay and the fibers and because they contain a higher percentage of fibers, see sample S5. The peaks shift due to the increase in the percentage of fiber. This may be due to better dispersion and exfoliation of the clay as a red brick building material. The FTIR results showed that the clay structure has a high porosity to reduce the thermal and acoustic flow. In the right part, we have added the absorption spectra to deduce that the absorbance decreases as a function of the percentage of fibers to 10%. Nevertheless, the fibers leave pores after the heat treatment of the brick.

FTIR analysis for functional groups revealed the presence of various characteristic functional groups in the samples of clay and clay doped by fibers. The frequency range and functional group obtained from transmittance spectra are presented in Table 2 (Bilgiç C. and Bilgic S., 2019; Chen et al., 2015)

Table 2. FTIR frequency range and functional groups present in the samples

Peak	**Transmittance (%)**	**Frequency range (cm^{-1})**	**Functional group**
		Raw clay	
1	89.26	446.51	Si-O stretching, Si-O-Fe Stretching
2	94.64	1006.87	Si-O-Si, Si-CH=CH_2: (C-H) trans waggin vibration Si-O stretching
Peak	**Transmittance on (%)**	**Frequency range on (cm^{-1})**	**Functional group**
		Clay + 2.5% of Fibers	
1	-	-	-
2	97.92	1000.15	Si-O-Si, Si-CH=CH_2: (C-H) trans waggin vibration. Si-O stretching
Peak	**Transmittance (%)**	**Frequency range (cm^{-1})**	**Functional group**
		Clay + 5% of Fibers	
1	92.98	431.32	Si-O stretching, Si-O-Fe Stretching
2	97.28	1014.56	Si-O-Si, Si-CH=CH_2: (C-H) trans waggin vibration Si-O stretching
Peak	**Transmittance on (%)**	**Frequency range on (cm^{-1})**	**Functional group**
		Clay + 7.5% of Fibers	
1	88.15	445.99	Si-O stretching, Si-O-Fe Stretching
2	93.90	1007.04	Si-O-Si, Si-CH=CH_2: (C-H) trans waggin vibration Si-O stretching
Peak	**Transmittance (%)**	**Frequency range (cm^{-1})**	**Functional group**
		Clay + 10% of Fibers	
1	88.89	445.46	Si-O stretching, Si-O-Fe Stretching
2	94.19	1012.68	Si-O-Si, Si-CH=CH_2: (C-H) trans waggin vibration Si-O stretching

3.2. Scanning electron microscopy analysis

Scanning electron microscopy (SEM) images of different composition of composites as shown in Fig. 7A to 7F, there is a significant difference in morphology of the studied samples. The stark contrast between crystalline cellulose, modified clay, composite S1 and S6 are clearly visible from their SEM images at 8500× magnification. As can be seen from Fig. 7A to Fig. 7D, from the SEM images, it is evident that there is no separate cellulosic fiber visible in composite. Moreover, clay particles are not distinct either. In composite S1, the structure of the composite surface is compact. The surface is rough and porous. It is impossible to distinguish either cellulose or clay even at 1000× magnification. Cellulose fiber has changed its structure. Instead of fibrous structure, it looks more like slates here. In composite S5, with 15% crystalline cellulose, the structure is more filled and less porous. It is difficult to separate individual particles. The structure looks layered with smoother surface. The surface of the clay doped with 2.5% of fibres as shown in Fig. 7A is coarse and rough. There are a few non-uniform aggregates on the surface. The surface is characterised with heterogeneous non-uniform particles, which dye molecules can adhere to. There are also holes on the surface that can encapsulate (Sathish et al., 2021; El-Hami, 2022).

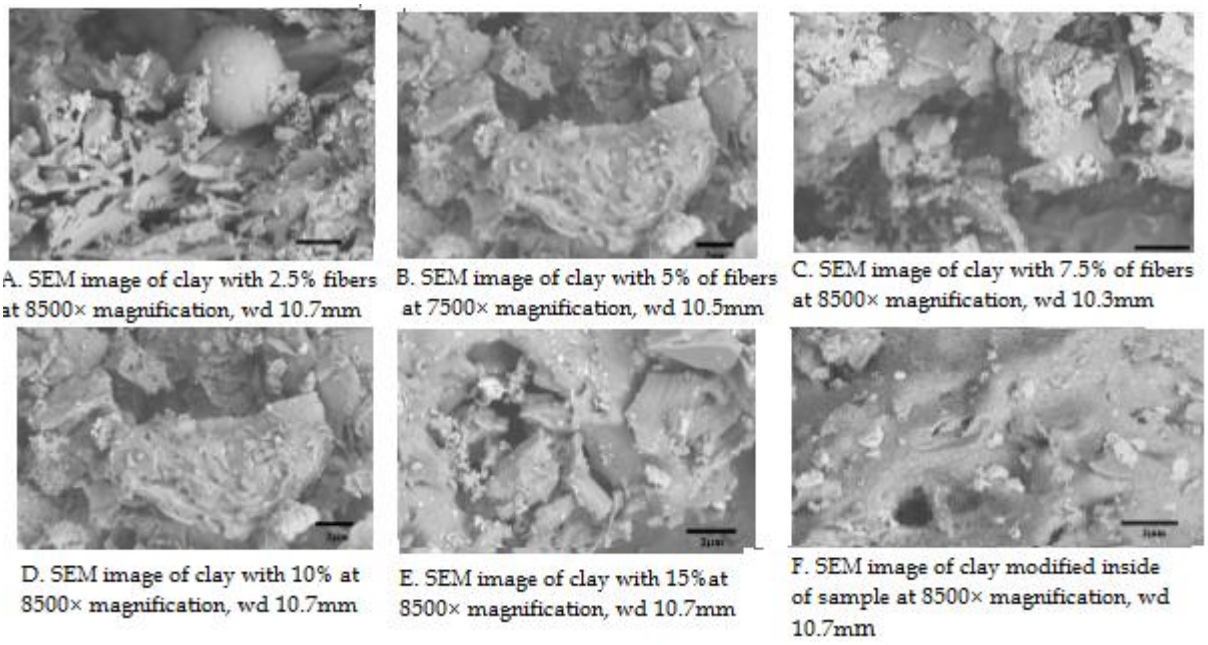

Fig. 7. SEM images of clay doped by different percentage of fibers

3.3. X-ray diffraction (XRD)

XRD analysis is most commonly used to determine the crystallinity and physical structure of the sample after the modification. The Fig.8 exhibits the XRD pattern for raw and C8 treated of date palm Phoenix dactylifera fiber (DPF). The diffractogram of raw and C8 treated of date palm Phoenix dactylifera fiber (DPF) shows two peaks commonly seen in DPF (Sathish et al., 2021; Bezazi et al., 2020; Perera et al., 2022). The first peak at (16.6°) corresponding to the 101 planes represents the presence of amorphous constituents of cellulose, hemicellulose and lignin. The second peak (23°) corresponds to the 200 plane represents the presence of α-cellulose (Sathish et al., 2021; Bezazi, et al., 2020; Perera, et al., 2022). The experimental results reveal that during surface treatments with fibers, there is no structural transformation from cellulose. The XRD diffraction pattern of clay doped by fibers of reed plant (Fig. 8) and the quantifcation data reveal that there are four major compounds (alumina, silica, calcite or calcium carbonate and burnt ochre or iron oxide) in the composite (Adebayo et al., 2021; Adebayo et al., 2020). The composite is dominated by calcite, followed by alumina, burn ochre, and silica. The assignments of the peaks are: alumina (Al_2O_3) with 2θ of 25.441° (0 1 2), 43.363° (1 1 3), and 54.574 ° (0 2 4) (JCPDS card: 00-010-0173); silica or quartz (SiO_2) with 2θ of 26.587° (1 0 1), and 45.809° (2 0 1) (JCPDS card: 00-033-1161); calcium carbonate ($CaCO_3$) with 2θ of 29.406° (1 0 4), 31.418° (0 0 6), and 50.319 ° (1 1 6) (JCPDS card: 00-005-0586); and iron oxide (Fe_2O_3) with 2θ of 33.134° (1 0 4), 35.752° (1 1 0), and 59.975 ° (1 1 3) (JCPDS card: 00-033-0664). The clay doped by fibers has high degree of crystallinity.

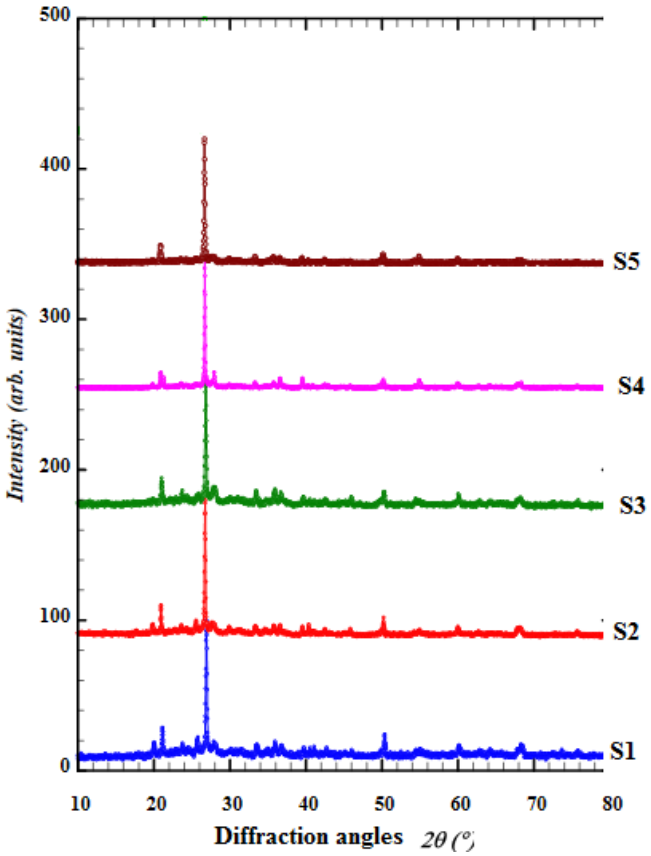

Fig. 8. XRD patterns for red brick doped by different percentage of reed fibers

3.4. X-Ray fluorescence spectroscopy

The percentage of silica and aluminium is very important for building and their application for red brick. This indicates the presence of kaolinite ($Al_2Si_2O_5(OH)_4$). As for calcium, which is relatively high, therefore this material is rich in calcite ($CaCO_3$). The alumina/silica ratio provides information on the permeability of the material humidity towards an increase pore size of structure for our focus to reduce the thermal and acoustic flow. The greater this ratio, the greater the permeability (Hartman et al., 2006). In our case, this ratio is small Al_2O_3/SiO_2=0.422. This low value is in agreement with the low percentage of humidity (1.41%) estimated by the loss on drying see table 3 (Jensen et al., 2018). The SiO_2/Al_2O_3 molar ratio = 2.3 (maximum substitution of Si^{4+} by Al^{3+} is greater than the conventional bentonite value, which is 2.7. This difference indicates the presence of free quartz in the clay fraction in large proportion (Sathish et al., 2021). From the Table 3, we notice that the percentage (%) of elements increases when we add the cellulosic fibers, we can see that the cellulosic fibers have been incorporated into the structure of the clay as shown in the Table 3.

Table 3. Elementary chemical composition of the clay sample

Compound S	Conc 1	Conc 2	Conc 3	Conc 4	Conc 5	Conc 6	Unit
MgO	0.906	2.224	2.287	2.541	2.218	2.204	
Al_2O_3	5.025	12.856	13.558	13.171	13.378	12.015	
SiO_2	12.157	30.459	32.279	32.813	32.266	29.359	
P_2O_5	0.204	0.394	0.381	0.356	0.355	0.331	
SO_3	0.579	1.228	0.507	0.82	0.457	0.196	%
K_2O	2.293	4.333	4.503	4.042	4.474	4.141	
CaO	1.714	2.833	3.068	2.708	2.992	3.021	
TiO_2	0.513	0.82	0.85	0.75	0.87	0.767	
Fe_2O_3	5.458	6.981	7.46	6.303	7.751	7.32	

3.5. Particle size analysis

The measurements are carried out on the fraction retained during the screening of the raw clays on the sieve less than 100 μm. This fraction is then suspended in a solution of sodium hexametaphosphate in a concentration of 1 g/L. The suspension thus obtained is introduced into a granuloma LA-920 laser beam of the HORIBA brand. The particle size distribution is derived from the interaction between a set of particles and the incident laser beam (Choubert et al., 1984; Guillemin and Houzay, 1982 ; Jabaloy et al., 2015).

The properties of good plasticity and high water absorption are related to the fraction of particle size less than 20 μm, which actually represents the clay fraction.

The particle size and particle size distribution of the different clay shades show:

- A relatively high fraction of average particles: fraction between 0.13 and 1 μm;
- An average fine particle fraction: < 0.13 μm;
- A very small fraction of coarse particles: > 1μm.

Table 4. The results of the particle size analysis of the fraction below 100 μm

Clay		
Diameter (μm)	Frequence (%)	Frequence cumulee (%)
0.131	0	0
0.150	0.104	0.104
0.172	0.186	0.290
0.197	0.297	0.586
0.226	0.421	1.007
0.259	0.623	1.630
0.296	0.732	2.362
0.339	0.789	3.151
0.389	0.812	3.963
0.445	0.769	4.732
0.510	0.709	5.442
0.584	0.686	6.128
0.669	0.692	6.820
0.766	0.748	7.568
0.877	0.870	8.437
1.005	1.073	9.510

4. Conclusions

The main conclusions of the study, is as follows: it is clear that the clay and the reed fibers can be successfully incorporated to make a composite of clay and their structure very porous. The FTIR and SEM and DRX study showed good incorporation and significant changes in their structure and the XRD diffraction pattern of clay doped by fibers of reed plant and the quantifcation data reveal that there are four major compounds (alumina, silica, calcite or calcium carbonate and burnt ochre or iron oxide) in the composite of red brick. The FTIR analysis for functional groups revealed the presence of various characteristic functional groups in the samples of clay and clay doped by fibers. In addition, even at different colours and rings variation of the starting components, the composite material was able to show improved properties, although better results were obtained in composite nanofibers where the percentage of cellulose was lower than that of clay. The structure of the composite surface is compact. The surface is rough and porous. It is impossible to distinguish either cellulose or clay even at 1000× magnification. Cellulose fiber has changed its structure. Instead of fibrous structure, it looks more like slates here. The fibers produced from cellulose nanofibers can be used for fiber reinforced strong and environmentally friendly composites. A measuring instrument has been building; it is able to give significant values of thermal and acoustic properties. A study will later provide a systematic overview of how cellulosic reed plant fibers that used to modify the morphology and the thermal and acoustic properties of material nanofibers.

References

ADEBAYO, M. A., ADEBOMI, J. I., ABE, T. O. & AREO, F. I (2020). *Removal of aqueous Congo red and Malachite green using Ackee apple seed–Bentonite composite*. Colloid Interface Sci. Commun. 38, 100311

ADEBAYO, M. A., AKANDE S. O., OLORUNFEMI A. D., AJAYI O. O., OREGE J. I. AND DANIEL E. F., (2021). *Equilibrium and thermodynamic characteristics of the corrosion inhibition of mild steel using sweet prayer leaf extract in alkaline medium*. Prog. Chem. Biochem. Res. 4, 80–91

ALTINTIG, E., YENIGUN M., SARI A., ALTUNDAG H., TUZEN M., SALEH T. A., (2020). *Facile synthesis of zinc oxide nanoparticles loaded activated carbon as an eco-friendly adsorbent for ultra-removal of malachite green from water*. Environ. Technol. Innov. 21, 101305

ATIQAH,A.,JAWAID,AND AL (2018). *Effect of alkali and silane treatments on mechanical and interfacial bonding strength of sugar palm fibers with thermoplastic polyurethane.* J. Nat. Fibers 15(2), 251–261

AZIZI SAMIR MAS, ALLOIN F, DUFRESNE A (2005). *Review of recent research into cellulosic whiskers, their properties and their application in nanocomposite field.* Biomacromolecules 6, 612-626.

BASALEH, A. A., AL-MALACK, M. H. & SALEH, T. A (2019). *Methylene blue removal using polyamide-vermiculite nanocomposites: Kinetics, equilibrium and thermodynamic study*. J. Environ. Chem. Eng. 7, 103107

BEZAZI,A., Boumediri,H., GarciadelPino, G.,Bezzazi, B., Scarpa, F., Reis, P.N., & Dufresne, A., (2020). *Alkali treatment effect on phys- icochemical and tensile properties of date palm Rachis fibers*. J. Nat. Fibers. 1–18

BILGIÇ, C., BILGIC S. (2019). *Application of Fourier Transform Infrared (FTIR) Spectroscopy to Analysis of Clays.* Nevşehir Journal of Science and Technology, 8, 37-46.

CHEN CADC (2003). *Processing and Morphological Development of Montmorillonite Epoxy Nanocomposites.* Nanotechnol 14, 643-648.

CHEN CAN, JIA ZHIDONG, WANG XILIN, LU HAI, GUAN ZHICHEN, YANG CUIRU. (2015). *Micro Characterization and Degradation Mechanism of Liquid Silicone Rubber Used for External Insulation. Dielectrics and Electrical Insulation, IEEE Transactions on*. 22. 313-321.

CHENG D1, XIA H, CHAN HS (2005). *Synthesis and characterization of surfacefunctionalized conducting polyaniline-chitosan nanocomposite.* J Nanosci Nanotechnol 5: 466-473. [Crossref]

CHOI HJ, KIM SG, HYUN YH, JHON MS (2001). *Preparation and rheological characteristics of solvent-cast poly (ethylene oxide)/montmorillonite nanocomposites.* Macromol Rapid Commun 22, 320-325.

CHOUBERT, G. & FAURE-MURET, A. & HILALI, E.A. & HOUZAY, J.P. & LAMOTTEFRIZON, D.. (1984). *Carte géologique du Rif, échelle 1/50000, feuille Boudinar*. Notes et Mémories du Service Géologique du Maroc.

DRZYMALA, J., 2007. *Mineral processing. Foundations of theory and practice of minerallurgy.* Ofic. Wyd. PWr, Wroclaw, Poland.

EL-HAMI K., (2022). *Morphological Rearrangement of P(VDF-TrFE)/SWCNT Nano-composite Under High Electron Beam*. Springer Nature Switzerland AG 2022, AI2SD 2020. AISC 1418, 661–664.

GUILLEMIN, M. AND HOUZAY, J.P. (1982). *Le Néogène post-nappe et le Quaternaire du Rif nord-oriental. Stratigraphie et tectonique des bassins de Melilla, du Kert, de Boudinar et du piedmont des Kebdana*. Notes et Mémoires du Service géologique du Maroc, 314, 7-239.

HARTMAN J., ALBERTSSON A. C., SODERQVIST L. M., SJOBERG J., (2006). *Oxygen barrier materials from renewable sources: material properties of softwood hemicellulose-based films*. Journal of applied polymer science. Vol. 100(4), 2985-2991.

IOELOVICH M (2008). *Cellulose as a nanostructured polymer: a short review.* BioResources 3, 1403-18.

JABALOY, ANTONIO & AZDIMOUSA, ALI & BOOTH-REA, GUILLERMO & ASEBRIY, LAHCEN & VÁZQUEZ, MERCEDES & MARTÍNEZ-MARTÍNEZ, JOSÉ & GABITES, JANET. (2015). *The structure of the Temsamane fold-and-thrust stack (eastern Rif, Morocco): Evolution of a transpressional orogenic wedge*. Tectonophysics. 663. 10.1016/j.tecto.2015.02.003.

JENSEN J. L., CHRISTENSEN B. L., SCHJONNING P., WATTS C. W. AND MUNKHOLM L. J., (2018). *Converting loss-on-ignition to organic carbon content in arable topsoil: pitfalls and proposed procedure.* Journal of soil science, 69(4), 604-612.

Kbiri Z., El Ouai D., Tbib B., and El-Hami K., (2022). *Advanced Characterizations of Moroccan Clay Related to the Local Geology*. Springer Nature Switzerland, AG 2022, AI2SD 2020, AISC 1417, 796–800.

KBIRI Z., TBIB B., EL-HAMI K. *Influence of temperature in Properties of Clay for two zones in Morocco BeniYakhlef and Ben Slimane.* Springer Nature Switzerland AG 2020, AISC 1103, 193–198.

LI P, PING ZHENG J, LU MA Y, DE YAO K (2003). *Gelatin/montmorillonite hybrid nanocomposite. II. Swelling behavior.* J Appl Polym Sci 88, 322-326.

LU H, HU Y, YANG L, WANG Z, CHEN Z, ET AL. (2005). *Preparation and thermal characteristics of silane-grafted polyethylene/montmorillonite nanocomposites.* J Mater Sci 40, 43-46.

MAITI PB, CA GIANNELIS , E.P. (2003). *Renewable plastics: synthesis and properties of PHB nanocomposites.* Polym Mater Sci Eng 88, 58-59.

MCCORMICK C (2010). *Nanocellulose steps up on stage.* Pulp Paper-Canada 111, 15-16.

MESSERSMITH PBAEPG (1994). *Synthesis and characterization of layered silicate-epoxy nanocomposites.* Chem Mater 6: 1719-1725.

MINHAJUL I. MD., NURUZZAMAN KHAN M., BISWAS S., CHOUDHURY T. R., HAQUE P., RASHID T. U., MIZANUR R. M., (2017). *Preparation and characterization of bijoypur clay-crystalline cellulose composite for application as an adsorbent.* Adv Mater Sci, Volume 2(3), 1-7

MUTUTUVARI TM, TRAN CD (2014). *Synergistic adsorption of heavy metal ions and organic pollutants by supramolecular polysaccharide composite materials from cellulose, chitosan and crown ether.* J Hazard Mater 264, 449-459. [Crossref]

NGAH WW, HANAFIAH MAKM (2008). *Removal of heavy metal ions from wastewater by chemically modified plant wastes as adsorbents: a review.* Bioresour Technol 99, 3935-3948.

OKAMOTO M, MORITA S, KIM Y, KOTAKA T, TATEYAMA H (2001). *Dispersed structure change of smectic clay/poly (methyl methacrylate) nanocomposites by copolymerization with polar comonomers.* Polym 42, 1201-1206.

OLUSEGUN, S. J. &MOHALLEM, N. D. S (2020). *Comparative adsorption mechanism of doxycycline and Congo red using synthesised kaolinite supported $CoFe_2O_4$ nanoparticles*. Environ. Poll. 260, 114019

OUSHABI, A., OUDRHIRI HASSANI F., ABBOUD Y., SAIR S., TANANE O. AND EL BOUARI A., (2018). *Improvement of the interface bonding between date palm fibers and polymeric matrices using alkali-silane treatments.* Int. J. Ind. Chem. 9(4), 335–343

PARK H-M, LIANG X, MOHANTY AK, MISRA M, DRZAL LT (2004). *Effect of Compatibilizer on Nanostructure of the Biodegradable Cellulose Acetate/Organoclay Nanocomposites.* Macromolecules 37, 9076-9082.

PARK H-M, MOHANTY A. K., DRZAL L. T., LEE E., MIELEWSKI D. F., MISRA M., (2006). *Effect of Sequential Mixing and Compounding Conditions on Cellulose Acetate/Layered Silicate Nanocomposites.* Journal of Polymers and the Environment 14, 27-35.

PARK JH, JANA SC (2003). *Mechanism of exfoliation of nanoclay particles in epoxy-clay nanocomposites.* Macromolecules 36, 2758-2768.

PERERA, H. J., GOYAL, A., & ALHASSAN, S. M (2022). *Morphological, structural and thermal properties of silane-treated date palm fibers*. J. Nat. Fibers 1–11

RAY SS, BOUSMINA M (2005). *Biodegradable polymers and their layered silicate nanocomposites: in greening the 21st century materials world.* Progress in Materials Science 50, 962-1079.

RAY SS, YAMADA K, OKAMOTO M, UEDA K (2003). *Control of biodegradability of polylactide via nanocomposite technology.* Macromol Mater Eng 288, 203-208.

REIS, G. S., ADEBAYO, MATTHEW A., SAMPAIO, CARLOS H., EDER C., PASCAL S., IRINEU A. S., SILVIO L. P., & FLAVIO A., (2017). *Removal of phenolic compounds using sludge-based activated carbons prepared by conventional and microwave-assisted pyrolysis*. Water Air Soil Poll. 228(33), 1–17

SATHISH, S., KARTHI N., PRABHU L., GOKULKUMAR S., BALAJI D., VIGNESHKUMAR N., AJEEM FARHAN T.S., AKILKUMAR A., DINESH V.P., (2021). *A review of natural fiber composites: Extraction methods, chemical treatments and applications.* Mater. Today Proc. 45, 8017–8023

Smilja Markovic, Vera Dondur, Radovan Dimitrijevic (2003). *FTIR spectroscopy of framework aluminosilicate structures: carnegieite and pure sodium nepheline*. , 654(1-3), 223–234.

THIRUMAVALAVAN M, LAI Y-L, LIN L-C, LEE J-F (2009). *Cellulose-based native and surface modified fruit peels for the adsorption of heavy metal ions from aqueous solution: Langmuir adsorption isotherms.* J Chem Eng Data 55, 1186-1192.

WANG X, DU Y, LUO J, LIN B, KENNEDY JF (2007). *Chitosan/organic rectorite nanocomposite films: Structure, characteristic and drug delivery behaviour.* Carbohydr Polym 69, 41-49.

ZHUANG H, ZHENG JP, GAO H, DE YAO K (2007). *In vitro biodegradation and biocompatibility of gelatin/montmorillonite-chitosan intercalated nanocomposite.* J Mater Sci Mater Med 18, 951-957.